Journal of Materials Chemistry A

Accepted Manuscript

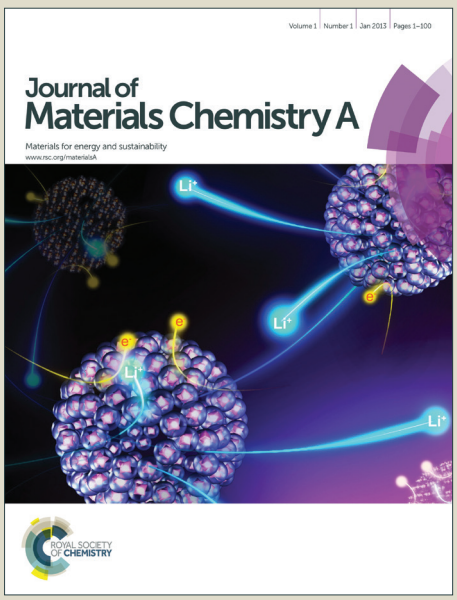

ROYAL SOCIETY OF CHEMISTRY

www.rsc.org/materialsA

Journal of Materials Chemistry A

Cite this: DOI: 10.1039/c0xx00000x

www.rsc.org/xxxxxx

PAPER

Rapid Synthesis of Mesoporous $Ni_xCo_{3-x}(PO_4)_2$ hollow Shells Showing Enhanced Electrocatalytic and Supercapacitor Performances

Jingchao Zhang, Yong Yang, Zhicheng Zhang, Xiaobin Xu, Xun Wang*

Received (in XXX, XXX) Xth XXXXXXXXX 20XX, Accepted Xth XXXXXXXXX 20XX
DOI: 10.1039/b000000x

Design cost-effective electrocatalysts and supercapicitor electrode materials with delicate hierarchical morphologies and enhanced functionalities are amazing in energy conversion and storage processes. Here, a fast and efficient microwave-assisted oil-in-water microemulsion template hydrothermal method is applied for the synthesis of multiple components and functional mesoporous hollow $Ni_xCo_{3-x}(PO_4)_2$ shells. Due to the high surface areas and correspondingly increased electroactive sites derived from the mesoporous and hollow characteristics, the obtained $Ni_xCo_{3-x}(PO_4)_2$ shells exhibit excellent performance as nonenzymatic glucose sensor, nonprecious electrocatalyst for oxygen evolution reaction (OER), and electrode materials in energy storage.

Introduction

Hollow nano-sized structures with inner cavities and functional shells have attracted increasing attentions because of their wide potential applications in absorption and separation, chemical sensors, catalysis, drug carriers, energy storage, and confined nanoreactors.[1] Particularly, mesoporous hollow shell structures with proper pores in 2~5 nm can provide more electroactive sites and short diffusion paths for charge carriers,[2] which may endow the materials with enhanced electrochemical properties. To date, various chemical methods have been developed to prepare hollow structures including sacrificial template route, galvanic replacement, Kirkendall effect, and Ostwald ripening process.[3] However, it still remains challenging to synthesize mesoporous hollow shells with large void space to maximize the amount of active surface, especially for multi-component compounds with delicate mesoporous hollow morphologies and enhanced functionalities.

Recently, increasing attentions have been paid to the development of Co, Ni-based or ternary Ni-Co oxides, sulfides, and layered double hydroxides due to their high electrochemical activities as electrode materials in supercapacitors[4] or as electrocatalysts in splitting water.[5] It would therefore be desirable to synthesize ternary Co-Ni-based shells with mesoporous inner structures under mild conditions, the three dimensional-available active sites of which may make them ideal candidates as electrocatalysts substituted for expensive enzymes and precious metals.

Herein, we described a facile route to synthesize mesoporous $Ni_xCo_{3-x}(PO_4)_2$ series hollow shells in a mixture boiling solution under 185 ^oC which generated stable oil-in-water emulsions. The as-made $Ni_xCo_{3-x}(PO_4)_2$ hollow shells display excellent multiple electrochemical properties including supercapacitors, electrochemical sensors and OER electrocatalysts. The constructed amperometric sensor from the combination of mesoporous $Co_3(PO_4)_2$ shells with traditional electrode showed a linear range for the detection of glucose from 2.5 to 312 μM with a correlation coefficient of 0.9926, which as an artificial glucose oxidase mimic decreased the cost and simplified the complex electrode fabrication process with the immobilization of glucose oxidase.[6] Moreover, the 3D mesoporous $NiCo_2(PO_4)_2$ shells, which may be a good candidate of electrochemical capacitors with a high specific capacitance up to 940 F g^{-1} at a current density of 1 A g^{-1} and a long cycle life which can maintain 85% of initial specific capacitance after 1000 cycles at a current density of 4 A g^{-1}. Meanwhile, the low-cost $NiCo_2(PO_4)_2$ with rich porosity and hierarchical hollow structures also shows a lower overpotential at ~0.34 V after 2 h cycling at 10 mA cm^{-2} and a reduced Tafel slope of 35 mV/dec lower than that of the Ir/C catalyst (40 mV/dec),[5b, 7] which is attractive targets in oxygen evolution reactions.

Results and discussion

Scheme 1 shows the synthetic strategy for the mesoporous $Co_3(PO_4)_2$ hollow shells using oil-in-water emulsion as soft template. Oil-in-water emulsion was formed by suspending hexane droplets in water and N, N-dimethylacetamide (DMA) interface. Because of the good miscibility of DMA and water, hexane is easy to be encapsulated into water and then formed the oil-in-water emulsions. Triethylamine may act as a capping reagent added to stabilize the oil-in-water emulsions and facilitate the formation of hollow $Co_3(PO_4)_2$ shells. The stable emulsions play a crucial role in producing mesoporous hollow shell structures, with their surfaces or bodies serving as structural templates and guaranteeing the nuclear and self-assembly process of the reactants at the two phase interface.[8] Due to the

introduction of microwave-assisted method to this strategy,[9] all the reactions can be finished within 20 minutes, which may provide an efficient way for large scale production. To understand the formation of hollow and mesoporous shells during the synthesis, a series of control experiments were conducted using the standard procedure. With the absence of either triethylamine or hexane, no void structure could be found in the products. Corresponding resultant products consist of short nanowires assembled from small hollow nanoparticles (Fig. S1a) and irregular nanosheets (Fig. S1b), respectively. The above results indicated that the morphologies of the products can be facilely controlled by adjusting the amount of capping agent and the ratio of metal ions in the initial stage.

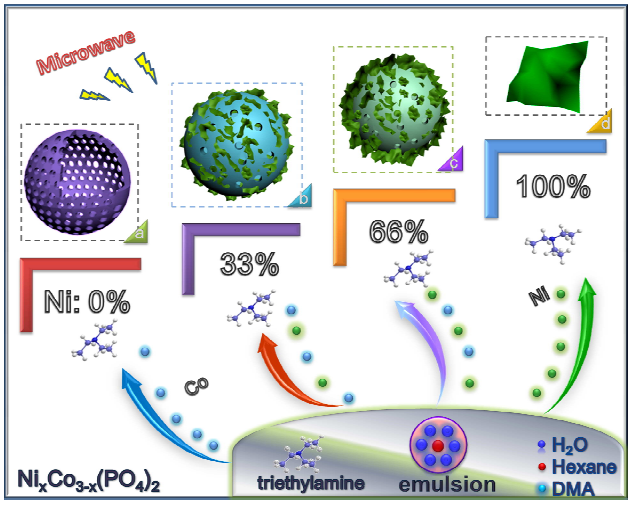

Scheme 1 Illustration of the possible process for the formation of $Ni_xCo_{3-x}(PO_4)_2$: (a) $Co_3(PO_4)_2$ mesoporous hollow shells obtained in oil-in-water emulsion with the assistant of triethylamine in the synthetic system. (b) Pompon-shaped $NiCo_2(PO_4)_2$ hierarchical shells doped by 33% Ni ions. (c) Mesoporous $CoNi_2(PO_4)_2$ hierarchical shells doped by 66% Ni ions. (d) $Ni_3(PO_4)_2$ nanosheets with 100% Ni substitution.

The materials isolated during the synthetic processes were investigated by transmission electron microscopy (TEM) and scanning electron microscopy (SEM). According to TEM studies in Fig. 1a and Fig. S1, these hollow shells have a size distribution in the range of 200~600 nm，the average size is ~300 nm. The hollow structure was further proved by the obvious contrast between the well-defined shells and the large inner void cavities, and especially clearly shown by a broken spherical shell inset in Fig. 1a. Energy-dispersive X-ray (EDX) mapping analysis confirms the even distribution of Co, P, O elements in the shells (Fig. 1b). With a closer examination, the dark field scanning TEM (STEM, Fig. 1b, S1f) and the TEM observation of a single sphere (Fig. 1 c) were also conducted, which reveal the porous and hollow shell architecture. The analysis of N_2 sorption isotherms based on the Brunauer-Emmet-Teller (BET) theory shows mesoporosity and high surface area of the $Co_3(PO_4)_2$ hollow spherical shells about 171 $m^2 g^{-1}$ and the average pore diameters of the hollow shell is ~3.7 nm (inset in Fig. 1d). The high BET surface area and mesoporous structure of the hollow $Co_3(PO_4)_2$ shells provide the possibility of efficient transport of electrons and ions, leading to high electrochemical activities of this electrode material.

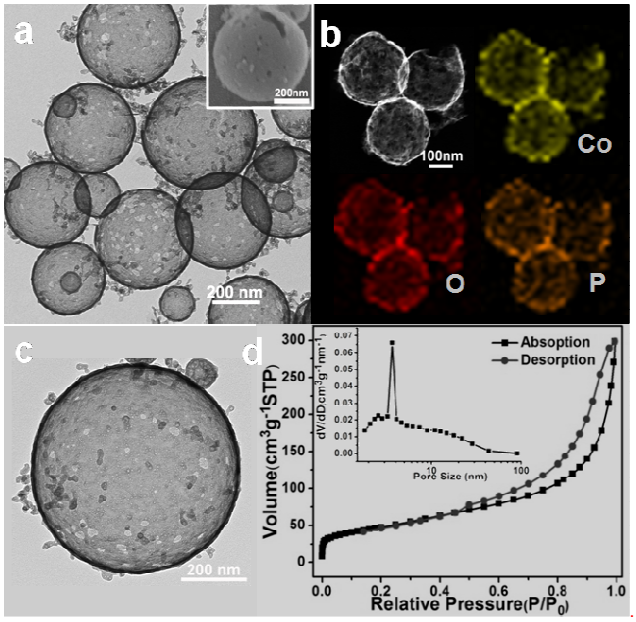

Fig. 1 (a) High magnification TEM image of mesoporous $Co_3(PO_4)_2$ hollow shells prepared at 185 °C under the irritation of microwave for 20 min, inset is the SEM image of a cracked single shell with hollow cavity inside. (b) STEM image and EDX elemental maps of the $Co_3(PO_4)_2$ hollow shells. (c) TEM image of a single $Co_3(PO_4)_2$ hollow shell which clearly indicated the porous structure. (d) Nitrogen adsorption-desorption isotherm, inset is the BJH pore size distribution plot of the $Co_3(PO_4)_2$ hollow shells.

Fig. 2a-c and Fig. S2 also show the representative TEM images of as-prepared $Ni_xCo_{3-x}(PO_4)_2$. Impressively, when $Co(acac)_2$ was partial replaced by $Ni(acac)_2$ and keep other experimental conditions unchanged, pompon-shaped hollow shells were formed (x>0.75). Taking $NiCo_2(PO_4)_2$ hollow shells as a sample, TEM observation reveals that the hierarchical hollow particles with relatively thin shells (~ 5 nm) are covered by ultrathin nanosheets, as shown in Fig. 2c. TEM images in Fig. S2 reveal the preferred growth of the hollow shells after microwave irradiation for 1 min. While, ultrathin nanosheets first appear at microwave irradiation for 5 min, and the number of nanosheets increase with extension the reaction time. The above results indicate that the prior formed hollow shells can be served as self-template and facilitate the assembly of nanosheets. EDX mapping analysis shows the existence of Ni, Co, P, O elements in the pompon-shaped hollow shells obtained at microwave irradiation for 20 min (Fig. S3). The non-uniform spatial distribution of Ni and Co elements between the shell and inside cavity was further manifested by the line scan profile of an individual $NiCo_2(PO_4)_2$ hollow shell (Fig. 2d-e). Moreover, the shape and composition of $Ni_xCo_{3-x}(PO_4)_2$ can be further tuned by varying the Co/Ni molar ratio in the starting materials. TEM images coupled with detailed elemental make-ups (Fig. S4) reveal that more amount of flexible nanosheets were found to adhere to the outer surface of the mesoporous shell with a gradual increase of Ni content. After Co

is completely substituted by Ni, the pompon-shaped hollow shells eventually evolve into nanosheets.

The phase purity, crystal structure and chemical composition of the as-obtained products were further investigated by X-ray diffraction and EDS. XRD patterns of mesoporous hollow shells can be indexed to monoclinic phase $Co_3(PO_4)_2$ (JCPDS No.:13-0503, Fig. S5). Corresponding EDS analysis of these hollow shells revealed the molar ratio of Co and P content was similar with the original ratio of reactant (Fig. S6). Meanwhile, the main diffraction peaks moved to a high degree when the lattice of Co ions in $Co_3(PO_4)_2$ shells were substituted by Ni ions, which was agree with the EDS results (Fig. S7). Specifically, proper Ni-doping can enlarge the specific surface area of mesoporous shells. Nitrogen adsorption and desorption isotherms and the corresponding Barrett-Joyner-Halenda (BJH) pore size distribution curves (Fig. 2f) indicated that the pompon-shaped hierarchical structure endow the $NiCo_2(PO_4)_2$ sample with a higher surface area of 206 m^2 g^{-1} with the main pore diameter distribution of 3.6 nm. Conversely, a lower surface area of 120 m^2 g^{-1} yield as the content of Ni ions varied from 33% to 66% (Fig. 2g). Concerning the coexistence of multiple oxidation state of Co-Ni based oxide such as $Ni_xCo_{3-x}PO_4$, X-ray photoelectron spectra (XPS) tests were typically conducted to the as-obtained $Co_3(PO_4)_2$, $NiCo_2(PO_4)_2$ and $CoNi_2(PO_4)_2$ samples, and the corresponding XPS data analysis were shown in Fig. 2h-i and Fig. S8. For the sample with 100% Co phosphate, two major peaks band energy at 781.5 and 797.5 eV is ascribed to Co $2p_{3/2}$ and Co$2p_{1/2}$ transition, respectively (Fig. 2h), with line broadening and doublet separation enhancement up to 16.0 eV.

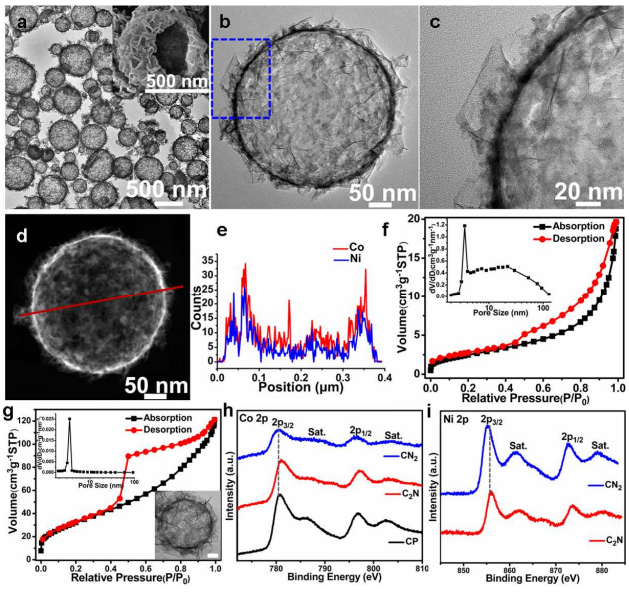

Fig. 2 (a-b) TEM images of pompon-shaped $NiCo_2(PO_4)_2$ hollow shells with different magnifications. (c) Magnified image of the selected area marked by dotted line in (b). (d) STEM image of a single $NiCo_2(PO_4)_2$ hollow shell and corresponding (e) EDX line scan profile for Co and Ni along the line as indicated in (d). (f) Nitrogen adsorption-desorption isotherm and BJH pore size distribution plot (inset) of pompon-shaped $NiCo_2(PO_4)_2$ hollow shells and (g) Mesoporous $CoNi_2(PO_4)_2$ hollow shells (inset is TEM image of a single shell, scale bar 50 nm). (h) XPS spectra of Co 2p for $Co_3(PO_4)_2$, $NiCo_2(PO_4)_2$ and $CoNi_2(PO_4)_2$ samples (labeled as CP, C_2N and CN_2, respectively) and (i) Ni 2p for $NiCo_2(PO_4)_2$ and $CoNi_2(PO_4)_2$ shells.

The Co 2p peak asymmetry may be the result of the overlapping of the intense lines for Co^{3+} and Co^{2+}. A strong shake-up satellite peak of Co $2p_{3/2}$ located at ~786 eV was also observed, which indicated surface enrichment of Co^{2+} ions in the 100% Co sample.[10] Remarkably, an apparent shift of the Co $2p_{3/2}$ to higher energy together with its flat and weak satellite peak for $NiCo_2(PO_4)_2$ demonstrated Co ions may donate electrons to Ni, simultaneously was mainly oxidized to Co^{3+}, which was further demonstrated by the increased portion of peak area in curve-fitting in Fig. S8. Comparatively, opposite shift followed by an enhancement of peak width and symmetry of Co $2p_{3/2}$ were also observed after 66% Ni doping, which may represent the majority of Co^{2+} ions present at the surface of $CoNi_2(PO_4)_2$ sample. Similarly, the aforementioned phenomena were also discovered in the high revolution XPS spectra of Ni $2p_{3/2}$, P 2p, and O 1s (Fig. 2i and Fig. S8). To same extend, the variable valency of Co and Ni ions in $Ni_xCo_{3-x}(PO_4)_2$ series is apt to affect the resistance of these samples (Fig. S8).

The electrochemical properties of the $Ni_xCo_{3-x}(PO_4)_2$ samples were firstly evaluated in low alkaline concentration. Compared with $NiCo_2(PO_4)_2$ and $CoNi_2(PO_4)_2$, cyclic voltammogram (CV) of mesoporous $Co_3(PO_4)_2$ shells shows the highest current density (Fig. S9), which may be preferred active material suitable for nonenzymatic glucose sensor. Fig. 3a shows the CV curves of the hollow $Co_3(PO_4)_2$ shells modified glass carbon electrode ($Co_3(PO_4)_2$/GCE) in the presence and absence of 5 mM glucose in 0.1 M NaOH. A couple of redox peaks occurred at the $Co_3(PO_4)_2$/GCE electrode in the background electrolyte at ~0.30 and ~0.16 V, which may be attributed to the electrochemical reaction between Co^{2+} and Co^{3+}. When glucose was added, a highly increased oxidation current was observed in the CV curve (solid line), indicating that the $Co_3(PO_4)_2$ modified GCE greatly improved the electrocatalytic oxidation of glucose. The glucose sensing performance of the shell-like $Co_3(PO_4)_2$-modified electrode was evaluated by amperometric measurements in a stirring NaOH solution at a fixed potential of ~0.6 V, where an increase in the voltammetric currents is observed with the repeated addition of with different concentrations (Fig. 3b). Upon successively addition of glucose to the homogeneously stirred 0.1 M NaOH solution, the oxidation peak current increased steeply and reached the steady-state current within 5 s, indicating fast response of the $Co_3(PO_4)_2$ modified GCE. Furthermore, the $Co_3(PO_4)_2$ shells modified GCE has shown a good linear relationship (correlation coefficient, R = 0.9926) between the amperometric current and the glucose concentration from 2.5 μM to 320 μM with the detection limit of 2.5 μM. The repeatability of the sensor to glucose was also examined (Fig. 3c) and the relative standard deviation (RSD) was 5.6% for ten successive determinations of 80 μM using the same electrode. It will be an attracting method if the sensor could be applied on the analysis of glucose in physiological samples. Ascorbic acid (AA), uric acid (UA), dopamine (DA), and NaCl are common interferences in the physiological samples. In order to evaluate the anti-interference ability of the $Co_3(PO_4)_2$ hollow shells modified electrode, the interference influence was also examined with 150 μM glucose in the presence of 5 μM AA, 10 μM DA, 50 μM UA, 50 μM NaCl, as shown in Fig. 3d, the addition of these interferents give rise to negligible current changes, indicating high anti-interference ability of the presented electrode. The stability of $Co_3(PO_4)_2$ shells modified electrode was also investigated by amperometric

measurement under a constant potential of 0.6 V for 3600 s. The current response to 20 μM glucose still maintained 95% of its original value (Fig. S10), revealing the high stability of the $Co_3(PO_4)_2$/GCE electrode.

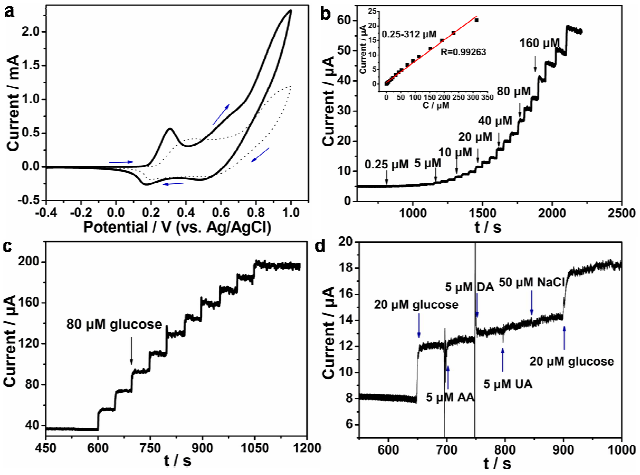

Fig. 3 (a) CV curves of $Co_3(PO_4)_2$/GCE in the absence (dotted line) and presence (solid line) of glucose in 0.1 M NaOH. (b) Amperometric sensing of glucose by successive addition of glucose at $Co_3(PO_4)_2$/GCE at 0.6 V in 0.1 M NaOH. Inset is plot of amperometric response versus the concentration of glucose from 2.5 μM to 320 μM. (c) Current-time curve of $Co_3(PO_4)_2$/GCE for successive addition of 80 μM glucose to stirred 0.1 M NaOH. (d) Interference test of $Co_3(PO_4)_2$/GCE with 20 μM glucose in the presence of 5 μM AA, 5 μM DA, 5 μM UA, and 50 μM NaCl.

Because the electrochemical capacitance is also proportional to the surface area of the electrode, the as-prepared porous $Ni_xCo_{3-x}(PO_4)_2$ series hollow shells with high surface area and hierarchical configuration was further investigated for supercapacitor application in high concentration alkaline solution (3 M). The CV experiments within a 0~0.5V range at a scan rate from 5 to 100 mV s^{-1} for the $NiCo_2(PO_4)_2$, $CoNi_2(PO_4)_2$ and $Co_3(PO_4)_2$ were presented in Fig. 4a, 4c and Fig. S11a. As shown in Fig. 4a, 4c, the CV curves were different from that of electric double-layer capacitance, suggesting that the capacity mainly results from pseudocapacitive capacitance. Obviously, a pair of peaks is visible in each voltammogram, indicating that the measured capacitance of $Ni_xCo_{3-x}(PO_4)_2$ hollow shells is mainly based on the surface reversible redox mechanism.[11] Furthermore, the existence of redox peaks at a scan rate of 50 mV s^{-1} indicated good rate performance of the $Ni_xCo_{3-x}(PO_4)_2$ series. Also, the shapes of the galvanostatic charge-discharge curves at different current densities are nearly symmetrical (Fig. 4b, 4d and Fig. S11b), demonstrating excellent electrochemical capacitive characteristics and reversibility of the redox reactions for these mesoporous $Ni_xCo_{3-x}(PO_4)_2$ hollow shells. The current-density dependence of specific capacitance is calculated from above discharge curves and plotted in Fig. 4e and Fig. S11c. Apparently, the hierarchical $NiCo_2(PO_4)_2$ hollow shells active electrode delivers the highest specific capacitance of 940.43, 918.14, 878.49, 799.19, and 765.29 F g^{-1} at current densities of 1, 2, 4, 8, and 10 A g^{-1}, respectively, compared to 638.15 to 514.98 and 239.31 to 188.89 F g^{-1} at the same current densities range for $CoNi_2(PO_4)_2$ and $Co_3(PO_4)_2$.

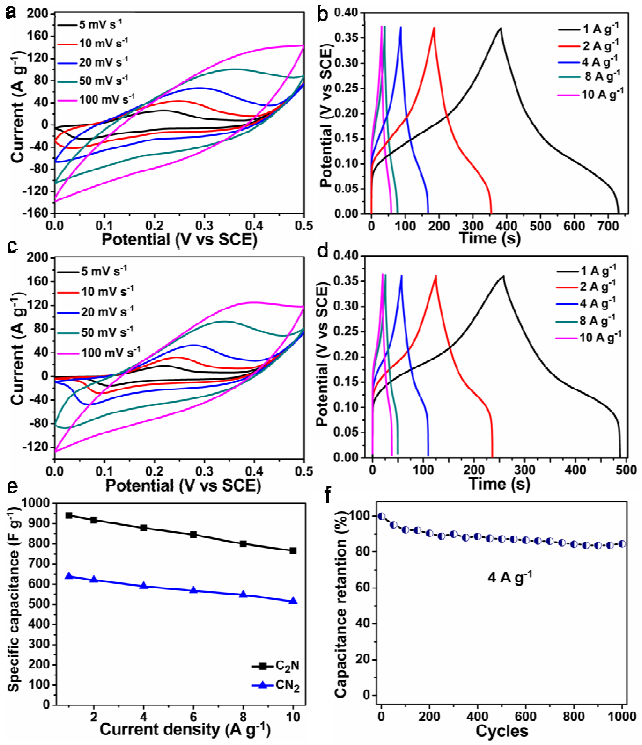

Fig. 4 Electrochemical performance characterization of mesoporous $Ni_xCo_{3-x}(PO_4)_2$ shells: (a) CV curves of mesoporous $NiCo_2(PO_4)_2$ shells modified electrode at various sweeping rates ranging from 5 to 100 mV s^{-1}. (b) Galvanostatic charge-discharge curves of $NiCo_2(PO_4)_2$ at different current densities. (c) CV curves of $CoNi_2(PO_4)_2$ shells modified electrode at various sweeping rates ranging from 5 to 100 mV s^{-1}. (d) Galvanostatic charge-discharge curves of $CoNi_2(PO_4)_2$ at different current densities. (e) Specific capacitance as a function of current density. (f) Cycling performance of $NiCo_2(PO_4)_2$ at a constant current density of 4 A g^{-1}.

Based on the BET results in Fig. 2f, the mesoporous $NiCo_2(PO_4)_2$ shells with the highest surface area may provide massive electroactive sites and more channels for electrolyte ions diffusion, which may enhance the travelling speed of the ions and thus bring higher specific capacitances. Compared with $NiCo_2(PO_4)_2$, remarkable reduction of surface area caused by the increased percentage composition of nickel ions is responsible for the decay of capacity for $CoNi_2(PO_4)_2$ sample. In addition, the $NiCo_2(PO_4)_2$ sample still retains the highest capacitance of ~81.4% after the current densities increasing from 1 to 10 A g^{-1}. Thus, such characteristics make it an ideal subject for further charge-discharge stabilization study. Impressively, $NiCo_2(PO_4)_2$ hollow shells possess high electrochemical stability for a long cycle life after 1000 repeating cycles with a total capacitance loss of about 15.5% at 4 A g^{-1} (Fig. 4f).

Most interesting and extraordinary is that besides the high performance of supercapacitors, $Ni_xCo_{3-x}(PO_4)_2$ hollow shells could operate in catalyzing the decomposition of water, which enlightened and manifested by the bubbles formed on nickel foam electrode of supercapacitors. We further investigated the

influence of the Ni ions doping on the electrocatalytic performance of oxygen evolution reaction (OER) using this series samples. One of benchmarks for an OER catalyst is the operating potential required to achieve a current density of 10 mA cm^{-2}, which is approximately the current density for a 10% efficient solar-to-fuel conversion device[12]. As shown in Figure 5a, the linear scan voltammograms (LSV) of $Ni_xCo_{3-x}(PO_4)_2$ hollow shells with same loading density of 0.12 mg/cm^2 were firstly examined. The current density was normalized to the geometric area and the measured potentials vs Hg/Hg_2Cl_2 (SCE) were converted to a reversible hydrogen electrode (RHE) scale according to the Nernst equation:

$$E_{RHE} = E_{SCE} + 0.059\ pH + 0.244 \quad (1)$$

the overpotential (η) was calculated according to the formula:

$$\eta\ (V) = E_{RHE} - 1.23 \quad (2)$$ [13]

In 1 M KOH, the pH value of the electrolyte was measured as 14.00. Remarkably, the operating potential of $NiCo_2(PO_4)_2$ hollow shell electrode was down to 1.577 V (vs E_{RHE}, η=347mV), comparable to or smaller than the overpotential of well-studied Co-based noble-metal free OER catalysts, for example, Co_3O_4/N-rmGo (0.31 V, 1M KOH), $Ni_xCo_{3-x}O_4$ nanowire arrays (0.379 V, 1M NaOH), and $Mn_3O_4/CoSe_2$ hybrids (0.45 V, 0.1M KOH), and even comparable to the potential of noble-metal catalysts, for example, IrO_2/C (1.60 V, 0.1M KOH), and IrO_2 nanoparticles (1.60 V, 0.5M H_2SO_4). [5a,14] At the same overpotential (η=0.35 V), the best performed $NiCo_2(PO_4)_2$ showed an approximately 8-fold higher current density than $CoNi_2(PO_4)_2$ (Fig. 5b). As is clearly shown, the proper addition of Ni can improve the electrochemical water splitting activity. Combined with the XPS results in Fig. S8, the high level of Co^{3+} in $Co_3(PO_4)_2$ or coexisting Co^{3+} and Ni^{3+} ions in $NiCo_2(PO_4)_2$ sample may facilitate to generate further oxidized Co^{4+} or Ni^{4+} species, which was believed to promote the intermediate catalytic process to produce O_2 and enhanced OER activity.[15] Taking surface area into consideration, the largest exposure of the surface Co and Ni of $NiCo_{3-x}(PO_4)_2$ samples may be essential to the electrochemical evolution of oxygen, leading to the best OER performance of $NiCo_2(PO_4)_2$. Besides, the Tafel slope is another key factor for the evaluation of OER kinetics, which is determined from curve fitting in the liner regions of polarization curves according to Tafel equation:

$$\eta = b \log j + a \quad (3)$$

When the Ni content is around 33%, the Tafel slope b reaches its optimal value at around 35 mV dec^{-1}, which was smaller than that of $CoNi_2(PO_4)_2$ (56 mV dec^{-1}) and $Co_3(PO_4)_2$ (84 mV dec^{-1}) (Fig. 5c), this result indicated that proper Ni doping may kinetically expedite the water-splitting reaction. In addition, the 33% Ni doped mesoporous $NiCo_2(PO_4)_2$ shells exhibited considerable catalytic durability. After 2 h of constant polarization at 10 mA cm^{-2}, the $NiCo_2(PO_4)_2$ catalyst had a gradually reduced overpotential with a minimum value of 336 mV (Fig. 5d), indicating the laudable activation of this material in alkaline electrolyte. Low overpotential, high catalytic current, small Tafel slope and low loading density indicate that $NiCo_2(PO_4)_2$ is a highly active non-precious metal OER electrocatalyst.

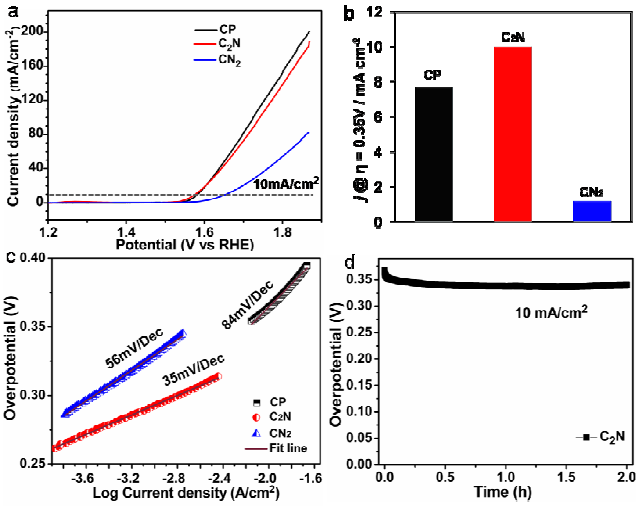

Fig. 5 (a) Polarization curves of $Co_3(PO_4)_2$, $NiCo_2(PO_4)_2$ and $CoNi_2(PO_4)_2$ catalysts in O_2-saturated 1 M KOH at a scan rate of 10 mV s^{-1} and a continuous electrode rotating speed of 1600 rpm. (b) Activity of the catalysts at an overpotential of 0.35 V. (c) Tafel plots of oxygen evolution reaction (OER) currents derived from (a). (d) 2-h controlled-current electrolysis at 10 mA cm^{-2} per geometric area for $NiCo_2(PO_4)_2$ electrocatalysts on glassy carbon supports.

Conclusions

In summary, the mesoporous shell-like $Ni_xCo_{3-x}(PO_4)_2$ hollow structures can be easily synthesized via one-pot oil-in-water emulsion method in a short time under microwave irradiation. The electrochemical measurements reveal that the as-prepared $Co_3(PO_4)_2$ mesoporous shells are attractive as electrode material for glucose detection with insignificant interference from ascorbic acid, uric acid and dopamine. Furthermore, the proper introduction of Ni dopants (33%) not only remarkable improved the electrochemical capacitance but also enhanced the electrocatalytic water-splitting performance with excellent activity and stability. The mesoporous $Ni_xCo_{3-x}(PO_4)_2$ shells electrode material with large specific surface area, permeable mesoporous thin walls, high electrocatalytic activity and stability combined with its low cost and facile synthesis suggests that it has potential applications in amperometric biosensors, energy storage and electrocatalysts in the future.

Experimental Section

Synthesis

In a typical procedure, cobalt (II) acetyl acetonate (0.0257g, 0.1mmol) was dispersed in triethylamine (0.75 mL), dimethylacetamide (4.0 mL), and a small amount of hexane (0.5 mL). And then, a large amount of disodium hydrogen phosphate aqueous solution (0.0238g/6.5 mL) was added to the mixed solution in turn to form a micelle system when stirring vigorously. The mixture was stirred for a few minutes, sealed and heated to 185 °C under the irritation of microwave, and maintained at this temperature for 20 min. Pompon-shaped $Ni_xCo_{3-x}(PO_4)_2$ shells were prepared by altering the molar ratio of cobalt (II) acetyl acetonate and nickel acetyl acetonate in the starting materials, and keep other reaction parameters unchanged. The obtained products were separated by centrifugation and washed by ethanol and water repeatedly, and finally dried in vacuum at 80 °C for 1h.

Characterization

The resultant phase of the hollow $Co_3(PO_4)_2$ shells was determined by X-ray diffraction (XRD, Cu 60 F Kα radiation, Rigaku D/max2550VB, Japan). The surface morphology was observed using scanning electron microscopy (SEM, LEO-1530, Germany). The morphology and microstructure was further studied by transmission electron microscopy (TEM, H7700, Hitachi, Japan) and high-resolution transmission electron microscopy (HRTEM, Tecnai G2, F20, 200 kV). The composition of the samples was analyzed by energy-dispersive X-ray spectroscope (EDX) attached to the TEM instrument. The specific surface areas of the samples were measured by N_2 adsorption measured using Micromeritics ASAP 2010M sorptionmeter. The XPS analyses were performed in a VG ESCALAB 200R spectrometer using monochromatic Al Kα radiation.

Electrochemical sensor electrode preparation and measurement

The electrochemical measurements were examined on an electrochemical workstation (CHI 760D, Chenhua, Shanghai, China) using a 3 mm GCE as working electrode, a platinum coil as counter electrode, and a Ag/AgCl electrode as reference electrode, respectively. To prepare the $Co_3(PO_4)_2$ modified electrode, 1.0 mg of the as-prepared product was dispersed in 1.0 mL water to give suspension by ultrasonicating. The bare glassy carbon electrode was successively polished with 1, 0.3, and 0.05 μm alumina slurry. A 5.0 μL of the suspension was dip-coated onto GC electrode and the electrode was then dried in the atmosphere. Glucose, uric acid, ascorbic acid, and dopamine were purchased from Aldrich.

Electrochemical supercapacitor electrode preparation and measurement

All the electrochemical experiments were carried out in a standard three-electrode system at room temperature. A saturated calomel electrode (SCE) and a platinum foil were used as the reference and counter electrodes, respectively. The working electrodes were typically fabricated by mixing 75% of active material, 15% of acetylene black, and 10% of polyvinylidene fluoride (PVDF), using N-methyl-2-pyrrolidone (Aldrich) as solution to yield a slurry. Then the slurry was pressed on the nickel foam current collector (1 cm × 1 cm) and dried in vacuum at 100 °C for 10 h. The actual mass loading of active material was 2.55 and 2.3325 mg for the $NiCo_2(PO_4)_2$ and $CoNi_2(PO_4)_2$ electrode, respectively. The electrochemical measurements were carried out by an electrochemical analyzer system, CHI 760D (Chenhua, Shanghai, China). The electrochemical performance of the electrode was analyzed using cyclic voltammetry (CV) and galvanostatic charge-discharge measurements in 3 M KOH aqueous solution in the potential window from 0 to 0.5 V.

OER electrocatalytic electrode preparation and measurement

5 mg catalyst powder was dispersed in the mixture of water and ethanol (v/v=3:1, 1 mL) with 50 μL Nafion solution under continuous ultrasonication at least for 30 min to form a homogenous ink. Next, 5 μL of the catalyst ink was transferred to a polished glass carbon electrode (5 mm diameter, 0.196 cm^2) with loading density of 0.12 mg/cm^2 and dried in nature. All the electrochemical tests were performed on PAR 4000 electrochemical workstation (Princeton Applied Research) at room temperature, using O_2 pre-saturated 1 M KOH solution as electrolyte. Pt film and Ag/AgCl were used as counter and reference electrodes, respectively. The linear sweep voltametry (LSV) curves were obtained at 1600 rpm, with a sweep rate of 10 mV/s. Electrochemical impedance spectroscopy (EIS) were carried out on PAR 2273 electrochemical workstation, the frequency scan range was from 100 kHz to 100 Hz. The pH value of 1 M KOH is ~14.00, which was measured by model PHS-25 pH meter (Shanghai Precision & Scientific Instrument CO.) All the OER catalytic measurements of $Ni_xCo_{3-x}(PO_4)_2$ samples were conducted with iR compensation enabled.

Notes and references

J. C. Zhang, Y. Yang, Z. C. Zhang, X. B. Xu, Prof. X. Wang
Department of Chemistry
Tsinghua University, Beijing, 100084, P. R. China
E-mail: wangxun@mail.tsinghua.edu.cn

† Electronic Supplementary Information (ESI) available: [details of any supplementary information available should be included here]. See DOI: 10.1039/b000000x/

1 a)X. W. Lou, L. A. Archer, and Z. Yang, *Adv. Mater.* 2008, **20**, 3987; b) Y. Li, J. Shi, *Adv. Mater.* 2014, **26**, 3176; c) K. Cheng, S. Peng, C. Xu, and S. Sun, *J. Am. Chem. Soc.* 2009, **131**, 10637; d) N. Kang, J. H. Park, M. Jin, N. Park, S. M. Lee, H. J. Kim, J. M. Kim, and S. U. Son, *J. Am. Chem. Soc.* 2013, **135**, 19115; e) G. D. Moon, J. B. Joo, M. Dahl, H. Jung, and Y. Yin, *Adv. Funct. Mater.* 2014, **24**, 848; f) B. Wang, J. S. Chen, H. B. Wu, Z. Wang, and X. W. Lou, *J. Am. Chem. Soc.* 2011, **133**, 17146; g) Q. H. Hong, X. F. Liu, Y. Fang, *Acta Chim. Sinica* 2013, **71**, 255; h) X. Fang, Z. Liu, M. F. Hsieh, M. Chen, P. Liu, C. Chen, and N. Zheng, *ACS Nano* 2012, **6**, 4434; i) R. J. Xing, A. A. Bhirde, S. J. Wang, X. L. Sun, G. Liu, Y. L. Hou, X. Y. Chen, *Nano Res.* 2013, **6**, 1.

2 S. Peng, L. Li, H. Tan, R. Cai, W. Shi, C. Li, S. G. Mhaisalkar, M. Srinivasan, S. Ramakrishna, and Q. Yan, *Adv. Funct. Mater.* 2014, **24**, 2155; J. C Chen, R. Y. Zhang, L. Han, B. Tu, D. Y. Zhao, *Nano Res.* 2013, **6**, 871.

3 a) C. Chen, W. Chen, J. Lu, D. Chu, Z. Huo, Q. Peng, and Y. Li, *Angew. Chem. Int. Ed.* 2009, **48**, 4816; b) J. Wang, N. Yang, H. Tang, Z. Dong, Q. Jin, M. Yang, D. Kisailus, H. Zhao, Z. Tang, and D. Wang, *Angew. Chem. Int. Ed.* 2013, **125**, 6545; c) N. Liu, Z. Lu, J. Zhao, M. T. McDowell, H. W. Lee, W. Zhao, and Y. Cui, *Nat. Nano.* 2014, **9**, 187; d) Y. Sun, and Y. Xia, *Science* 2002, **298**, 2176; e) M. H. Oh, T. Yu, S. H. Yu, B. Lim, K. T. Ko, M. G. Willinger, D. H. Seo, B. H. Kim, M. G. Cho, J.-H. Park, K. Kang, Y.-E. Sung, N. Pinna, and T. Hyeon, *Science* 2013, **340**, 964; f) Y. Yin, R. M. Rioux, C. K. Erdonmez, S. Hughes, G. A. Somorjai, and A. P. Alivisatos, *Science* 2004, **304**, 711; g) J. Huo, L. Wang, E. Irran, H. Yu, J. Gao, D. Fan, B. Li, J. Wang, W. Ding, A. M. Amin, C. Li, and L. Ma, *Angew. Chem. Int. Ed.* 2010, **49**, 9237. h) J. Nai, Y. Tian, X. Guan, and L. Guo, *J. Am. Chem. Soc.* 2013, **135**, 16082. i) T.Y. Ma, S. Dai, M. Jaroniec, and S. Z. Qiao, A*ngew. Chem. Int. Ed.* 2014, **53**, 7281.

4 a) L. Yu, L. Zhang, H. B. Wu, and X. W. Lou, *Angew. Chem. Int. Ed.* 2014, **53**, 3711; b) Y. Lei, J. Li, Y. Wang, L. Gu, Y. Chang, H. Yuan, and D. Xiao, *ACS Appl. Mater. Interfaces* 2014, **6**, 1773; c) J. Xiao, L. Wan, S. Yang, F. Xiao, and S. Wang, *Nano Lett.* 2014, **14**, 831; d) H. B. Wu, H. Pang, and X. W. Lou, *Energy Environ. Sci.* 2013, **6**, 3619. e) H. El-feky, M. Negem, S. Roy, N. Helal, A. Baraka, *Sci. China Chem.*2013, **56**, 1446; f) H. Tuysuz, Y. J. Hwang, S. B. Khan, A. M. Asiri, P. D. Yang, *Nano Res.* 2013, **6**, 47.

5 a) Y. Liang, Y. Li, H. Wang, J. Zhou, J. Wang, T. Regier, and H. Dai, *Nat. Mater.* 2011, **10**, 780; b) M. Gong, Y. Li, H. Wang, Y. Liang, J. Z. Wu, J. Zhou, J. Wang, T. Regier, F. Wei, and H. Dai, *J. Am. Chem. Soc.* 2013, **135**, 8452; c) M. Gao, W. Sheng, Z. Zhuang, Q. Fang, S. Gu, J. Jiang, and Y. Yan, *J. Am. Chem. Soc.* 2014, **136**, 7077; d) Z. Zhuang, W. Sheng, and Y. Yan, *Adv. Mater.* 2014, **23**, 3950; e) S. Chen, J. Duan, M. Jaroniec, and S. Z. Qiao, *Angew. Chem. Int. Ed.* 2013, **52**, 13567; f) Z. Zhao, H. Wu, H. He, X. Xu, and Y. Jin, *Adv. Funct. Mater.* 2014, DOI: 10.1002/adfm.201400118; g) X. Liu, Z. Chang, L. Luo, T. Xu, X.

Lei, J. Liu, and X. Sun, *Chem. Mater.* 2014, **26**, 1889; h) W. Zhou, X. J. Wu, X. Cao, X. Huang, C. Tan, J. Tian, H. Liu, J. Wang, and H. Zhang, *Energy Environ. Sci.* 2013, **6**, 2921; i) L. Kuai, J. Geng, C. Chen, E. Kan, Y. Liu, Q. Wang, and B. Geng, *Angew. Chem. Int. Ed.* 2014, **53**, 7547.

6 a) P. Si, S. Ding, J. Yuan, X. W. Lou, and D. H. Kim, *ACS Nano* 2011, **5**, 7617; b) B. Q. Yuan, C. Y. Xu, D. H. Deng, Y. Xing, L. Liu, H. Pang, and D. J. Zhang, *Electrochim. Acta* 2013, **88**, 708; c) Y. Guo, W. W. Li, M. Y. Zheng, Y. Huang, *Acta Chim. Sinica* 2014, **72**, 713; d) C. Guo, H. Huo, X. Han, C. Xu, and H. Li, *Anal. Chem.* 2013, **86**, 876.

7 a) X. Long, J. Li, S. Xiao, K. Yan, Z. Wang, H. Chen, and S. Yang, *Angew. Chem. Int. Ed.* 2014, **53**, 7584; b) G. J. Wang, F. Cheng, Y. Yu, C. Liang, T. Xu, M. Pan. *Sci. China Chem.* 2013, **56**, 131.

8 L. Chen, S. Yu, H. Wang, J. Xu, C. Liu, W. H. Chong, and H. Chen, *J. Am. Chem. Soc.* 2012, **135**, 835.

9 a) M. Baghbanzadeh, L. Carbone, P. D. Cozzoli, and C. O. Kappe, *Angew. Chem. Int. Ed.* 2011, **50**, 11312; b) I. Bilecka, and M. Niederberger, *Nanoscale* 2010, **2**, 1358.

10 a) F. B. Noronha, M. Schmal, B. Moraweck, P. Delichère, M. Brun, F. Villain, and R. Fréty, *J. Phys. Chem. B* 2000, **104**, 5478; b) J. G. Kim, D. L. Pugmire, D. Battaglia, and M. A. Langell, *Appl. Surf. Sci.* 2000, **165**, 70; c) Y. E. Roginskaya, O. V. Morozova, E. N. Lubnin, Y. E. Ulitina, G. V. Lopukhova, and S. Trasatti, *Langmuir* 1997, **13**, 4621.

11 C. Yuan, H. B. Wu, Y. Xie, and X. W. Lou, *Angew. Chem. Int. Ed.* 2014, **53**, 1488.

12 C. C. L. McCrory, S. Jung, J. C. Peters, and T. F. Jaramillo, *J. Am. Chem. Soc.* 2013, **135**, 16977.

13 S. Chen, and S. Z. Qiao, *ACS Nano* 2013, **7**, 10190; Z. Y. Liu, G. X. Zhang, Z. Y. Lu, X. Y. Jin, Z. Chang, X. M. Sun, *Nano Res.* 2013, **6**, 293.

14 a) M. R. Gao, Y. F. Xu, J. Jiang, Y. R. Zheng, and S. H. Yu, *J. Am.Chem. Soc.* 2012, **134**, 2930; b)Y. Li, P. Hasin, and Y. Wu, *Adv. Mater.* 2010, 22, 1926; c) Y. Zhao, R. Nakamura, K. Kamiya, S. Nakanishi, and K. Hashimoto, *Nat. Commun.* 2013, **4**, 2390; d) W. Hu, Y. Wang, X. Hu, Y. Zhou, and S. Chen, *J. Mater. Chem.* 2012, **22**, 6010.

15 a) M. W. Kanan, and D. G. Nocera, *Science* 2008, **321**, 1072; b) M. R. Gao, Y. F. Xu, J. Jiang, Y. R. Zheng, and S. H. Yu, *J. Am. Chem. Soc.* 2012, **134**, 2930; c) S. Chen, J. Duan, J. Ran, M. Jaroniec, and S. Z. Qiao, *Energy Environ. Sci.* 2013, **6**, 3693.